Conduction band electronic structure of metallic beryllium

V A Sashin†, M A Bolorizadeh†[§], A S Kheifets‡ and M J Ford†[*]

†School of Chemistry, Physics and Earth Science, Flinders University of South Australia, GPO Box 2100, Adelaide, SA 5001, Australia

‡Research School of Physical Sciences and Engineering, Institute of Advanced Studies, ANU, Canberra ACT 0200, Australia

Abstract. We have measured the bulk energy-momentum resolved density of the conduction band of metallic beryllium by means of electron momentum spectroscopy (EMS). From the data we have determined the band dispersion, occupied bandwidth, electron momentum density and density of states. The experimental results are compared with theoretical band structure calculations performed within the full potential linear muffin-tin orbital (FP-LMTO) approximation. There is good agreement between experiment and theory for the shape and intensity of the conduction band provided multiple scattering and hole lifetime effects are included. The measured occupied bandwidth is 11.15 ± 0.15 eV, which is larger than that predicted by our LMTO calculation, but agrees well with previous experimental and theoretical data. The experiment also reveals that the band dispersion is narrower in momentum compared to theory, the difference reaching as much as 0.15 a.u. near the Fermi momentum.

1. Introduction

Metallic beryllium occurs naturally in the hexagonal close packed structure with 8 electrons in the unit cell. The simplicity of this system lends itself to theoretical studies which it would be hoped can provide a complete description of its properties. In addition, Be is somewhat anomalous possessing the highest electron density among the simple metals and the largest deviation from free-electron like behavior.

Chemical bonding in Be exhibits covalent character with promotion of a valence *s*-like electron into an unoccupied *p*-like state. Hybridisation of the *s*- and *p*- states leads to formation of a wide *sp* band with metallic properties. This hybridisation is sufficiently strong that metallicity is preserved even when the lattice is expanded up to a factor of 1.6 times its equilibrium value[1]. Theoretical calculations (see, for example Chou *et al*[2]) predict the population of *2p*-like electrons in the ground state to be about twice as much as *2s*-like electrons. Similarly, experimental structure factors[3] and compton-scattering measurements[4] provide evidence of the covalent character and a 2p-like contribution to the wave function. Unlike most metals the density of states at the Fermi level in Be is very low and the Fermi surface is not spherical[5].

Numerous theoretical studies of the electronic structure of Be have been reported in the literature dating back to 1930[6]. The calculations have generally been assessed by comparison with experimental measurements of specific features of the band structure, such as special point energies and densities of states from X-ray emission data[7,8], and energy integrated momentum densities from compton scattering. An angle resolved photo-emission measurement (ARPES) has been reported which maps the full energy-momentum dispersion

§ Permanent address: Physics Dept., Shahid Bahonar University, Kerman, Iran.

relation[9]. A complete understanding of the peak intensities in ARPES measurements is, however, complicated by the electron and photon interaction processes involved and many-body effects in the initial and final states. In addition contributions from surface and bulk states alike must be considered in order to analyse the ARPES data.

In this paper we report on the conduction band electronic structure of metallic beryllium measured by electron momentum spectroscopy (EMS). EMS can provide a direct measurement of the full energy-momentum dispersion and band intensity, which compliments existing data to provide a thorough comparison with theoretical studies. The experimental results are compared to theoretical calculations in the linear muffin-tin orbital (LMTO) approximation. Multiple scattering effects present in the experiment are simulated in the LMTO calculation using a Monte Carlo procedure. The relative simplicity of metallic Be provides a strong incentive for these measurements in order to test our current theoretical understanding and resolve existing discrepancies with experiment.

2. Experimental

2.1. *(e,2e) spectrometer*

A description of the spectrometer used in the current work and its operation can be found elsewhere[10], here we limit ourselves to a brief outline.

The spectrometer measures electronic structure through the so-called (e,2e) reaction[11]. By means of this process the distribution of electrons in an atomic, molecular or

* Corresponding author. E-mail address: michael.ford@flinders.edu.au

solid target can be mapped in momentum space[12]. The abbreviation refers to electron impact ionization events where a high-energy incident electron transfers considerable momentum to the target. Under these conditions the (e,2e) collision can be regarded as a 'billiard-ball' like interaction between the incident and target electron. The energy and momentum of the incident electron beam is well defined in the spectrometer. By measuring completely the kinematics of the two outgoing electrons after the collision the target electronic structure is probed. In the plane-wave approximation the binding energy ε and momentum q of the target electron immediately before ionization can be determined by conversation of energy and momentum:

$$\varepsilon = E_0 - E_s - E_f \qquad q = p_s + p_f - p_0\,, \tag{1}$$

where ($E_{0,}$ p_0) refer to the energy and momentum of the incident electron, ($E_{s,}$ p_s) and ($E_{f,}$ p_f) are the same parameters for the two outgoing electrons. In the independent particle approximation the overall (e,2e) cross section as a function of energies and angles of the outgoing electrons is proportional to the absolute square of the target electron momentum space wavefunction, and gives the probability of finding the target electron with a particular momentum and binding energy.

Figure 1(a) shows schematically the scattering geometry of our (e,2e) spectrometer. As can be seen from the picture it exploits asymmetric non-coplanar kinematics. The incident and two outgoing electrons have nominally energies of 20.8, 19.6 and 1.2 keV respectively. The outgoing electrons are detected on the opposite side of the target from the incident beam. The detected electrons are accepted into the electrostatic energy analyzers at

polar angles of 13.6° and 76° relative to the direction of the incident beam. The entrance aperture of the fast electron analyzer accepts electrons over ±18° azimuthal angles relative to the *x*-*z* horizontal plane, and similarly the acceptance of the slow electron analyzer is ±6°. The overall momentum detection range with the above parameters is about ±3.5 a.u. The estimated resolution of the spectrometer is about 1 eV in energy and 0.15 a.u. in momentum. This resolution enables one to make a detailed energy-momentum mapping of valence electrons in solids that have a typical spread of a few eV in energy and of order 1 a.u. in momentum. In the absence of multiple scattering in the target (e,2e) events are only accepted where the target electron originally had its momentum directed along the *y*-axis. This feature provides the means to measure the electronic structure of crystalline targets in a particular direction. Coincidence detection of the two outgoing electrons supplies a very high level of sensitivity in the experiment, and is required to extract the true (e,2e) signal from a large background of other events.

An important advantage of the asymmetric geometry of the spectrometer is that it is sensitive to the surface layers of the target facing the slow electron analyzer. The escape depth of the slow electrons for most substances is about 2 nm meaning that the electronic structure information in our experiment comes predominantly from the outermost layers. Shading in figure 1(b) shows this schematically. Hence it is possible to perform measurements of targets prepared by evaporation onto a thin substrate, for instance, an amorphous carbon film. Ionization events taking place deeper within the target (non-shaded area) contribute mainly to the background intensity. The overall thickness of the target must be as small as possible in order to avoid the signal being dominated by multiple scattering[13].

The 2-nm sensitivity of the spectrometer has been exploited in the current work and our previous measurements of Mg / MgO[14] and Ca /CaO[30,15].

2.2. *Sample preparation and Characterization*

Beryllium targets are prepared *in situ* using a resistively heated evaporator. The metal in the form of flakes (99.5% purity, electrolytic) is evaporated onto 3 nm thick amorphous carbon (am-C) films which have previously been annealed to remove all impurities from the surface. Deposition rate and total thickness of the evaporated film are monitored by means of a quartz crystal microbalance. The base pressure in the evaporation chamber is about 10^{-10} Torr increasing during evaporation typically to a few times 10^{-8} Torr. A series of targets of different thickness ranging from 1 to 10 nm were prepared, a Be coverage of 3 nm was found to produce the optimal (e,2e) signal. The structure of the evaporated Be films is expected to be polycrystalline.

Be targets undergo chemical changes due to interaction with residual gases in the spectrometer chamber, mainly, water vapor[16]. Conduction band measurements were obtained by summing the initial data collection period for 5 separately prepared targets. This allows us to obtain data free of the effects of oxidation. The accumulated statistics totals about 1.5 million (e,2e) events at an average coincidence count rate of approximately 8 Hz, this is equivalent to a total measurement time of 50 hours.

Chemical composition of the target surface is monitored by means of Auger electron spectroscopy (AES). A typical Auger spectrum of a beryllium target measured just after deposition is presented in figure 2(a). The prominent Be KVV line is present over a smooth background with a small additional peak at about 270 eV which corresponds to the carbon

KLL line. The presence of this small carbon signal could be an indication of incomplete Be coverage of the substrate. However, the amount of carbon present on the surface from AES is negligible, and furthermore there is no carbon signal present in the (e,2e) data. In figure 2(b) the corresponding differential spectrum for an energy range around the Be KVV line is shown. The minimum observed at 105 eV due to the KVV transition in Be is in agreement with the literature value[17].

For further characterization we measure electron energy loss spectra at the two energies used in the (e,2e) measurement, namely 19.6 and 1.2 keV, with detection at 13.6^0 and 76^0 relative to the incident electron direction respectively. Electrons passing through the target experience multiple scattering predominantly small angle deflections and/or energy losses. The main mechanism of energy loss is through the excitation of collective oscillations of the conduction electrons with the transmitted electron losing an amount of energy characteristic of this plasmon excitation. Figure 3 shows the energy loss spectra of electrons passing through a 3 nm am-C + 3 nm Be film just after evaporation. The structure spanning 10 to 32 eV in figure 3(a) is the combination of a broad am-C bulk plasmon loss feature and a narrower Be bulk plasmon feature. The small bump on the low energy side of the broad structure can be ascribed to the surface plasmon in Be. For the slow electron shown in figure 3(b) the first and second order bulk plasmon energy losses in beryllium are clearly visible.

We have made a least squares fit to the spectrum in figure 3(a) to extract parameters for the energy loss features. The fitting function is a superposition of a linear background and three Gaussians, the am-C Gaussian having a fixed position and width of 22 eV and 17 eV respectively; these values are obtained from an independent fit to a pure am-C energy loss

spectrum. Solid lines in the graph represent the best fit to the Be energy losses and the dashed line is for the am-C energy loss. The position of the Be bulk plasmon is 19.6 ± 0.1 eV which taking into account dispersion of plasmon energy[18] is in reasonable agreement with the results of other authors[19,20]. Our halfwidth of 5.9 ± 0.3 eV also agrees well with existing data[21] considering that the measured plasmon intensity is integrated over a range of scattering angles and the halfwidth increases as the scattering angle increases[18]. The position and halfwidth for the Be surface plasmon are 13.2 ± 0.2 and 1.9 ± 0.5 eV respectively. The peak position is close to the free electron gas value of 13 eV, although Steiner *et al*[22,23] obtained a slightly smaller energy of 11.7 eV using XPS techniques. The measured halfwidth is considerably less than 14 ± 2 eV quoted by Steiner's group.

A similar fitting procedure has been applied to figure 3(b) using a linear function for the background and two Gaussians for the plasmon features. The position and halfwidth of the first order bulk plasmon agree within the experimental error with the values obtained above. The position and halfwidth of the second order bulk plasmon are 39.6 ± 0.2 and 10 ± 0.5 eV, respectively.

An independent estimate of the thickness of the evaporated Be layer can be obtained from the intensities of the plasmon peaks in figure 3(b). The probability of excitation of n plasmons is governed by a Poisson distribution:

$$P_n = e^{-x} (x^n / n!), \qquad (2)$$

where is x is the ratio of the thickness d to the mean free path for bulk plasmon excitation ì. In Be at the energy we employ for the slow electron, the expression by Quinn[24] gives value

of ì ~ 3.3 nm. The ratio, P_2 / P_1, of areas for the second and first plasmon peaks is 0.67 ± 0.08, giving a Be thickness of 4.4 ± 0.3 nm. Since the slow electron emerges from the target at 45^0 relative to the normal (see figure 1(b)) the found value is in good agreement with the value of 3 nm for the quartz crystal microbalance.

3. LMTO calculation

The band structure and the electron momentum density were calculated using the FP-LMTO method as described in Kheifets *et al*[25]. The experimental lattice parameters a = 2.2866 Å, c= 3.5833 Å were used, due to Wyckoff[26]. The local density approximation was employed with the Janak–Moruzzi–Williams parametrization to the exchange–correlation functional. The calculated band dispersions and electron momentum densities in several high-symmetry directions are shown in figure 4. We note that the Fermi level intersects the bands both in ΓM and ΓK directions, but not in ΓA direction. Near the Γ point only the lowest band is occupied, i.e. has a non-zero electron momentum density. The population switches to the next higher band in the second Brillouin zone. This population pattern forms a nearly continuous parabola except for small breaks at the Brillouin zone boundaries in ΓM and ΓK directions. These breaks, however, are washed out after spherical averaging which serves to simulate the polycrystalline nature of the sample.

4. Results and discussion

4.1. *Band Intensities*

The experimental energy-momentum resolved density of occupied states in the conduction band of metallic beryllium is presented in figure 5(a) as a gray-scale plot, darker color

representing higher density. Binding energies are relative to the vacuum level. The data have been binned into 0.4 eV and 0.1 a.u. energy and momentum intervals respectively. The free-electron-like parabola characteristic for dispersion in a metallic solid is distinctly visible. Since the sample is polycrystalline the measured density is a spherical average over all crystal directions. It is symmetric about zero momentum and disperses in binding energy from approximately 4 to 14.5 eV. The spread in momentum is about 1 a.u., in agreement with the free-electron value for the Fermi momentum of 1.03 a.u. The maximum intensity is not at the bottom of the conduction band at zero momentum, this effect is due to hole-lifetime broadening[27] which reaches a maximum at the band bottom.

At higher binding energies there is background intensity due to (e,2e) events where the electrons experience additional inelastic collisions. Darker areas mirroring the conduction band dispersion are observed at about 33 and 52 eV, these structures correspond to excitation of one or two plasmons, respectively. Additional intensity visible inside the conduction band parabola is the result mainly of elastic scattering of the electrons. The multiple scattering processes are detrimental to band density determination as they smear out the true occupied density. For this reason it would seem reasonable to minimize the thickness of the beryllium layer to 2 nm (the sensitivity of our spectrometer), however a 3-nm layer gives better suppression of the (e,2e) signal coming from the carbon substrate. Metals and semiconductors, with small or no band gap, generally have higher probabilities for inelastic multiple scattering at small energy losses compared to insulating materials that have wide band gaps. Our previous measurements illustrate this quite clearly[15,14,28].

Figure 5(b) shows the spherically averaged LMTO calculation convoluted with the experimental resolution (1 eV for energy and 0.15 a.u. for momentum). The binding energy

is shifted by approximately 4 eV to match the experimental energy of the conduction band minimum. The LMTO parabola is narrower than experiment and reaches a maximum at the band minimum, gradually decreasing as the momentum increases. After inclusion of finite hole-lifetime broadening these differences disappear and the calculated and measured band structures become very similar. This is demonstrated in figure 5(c) where the LMTO density is additionally convoluted with the hole lifetimes extracted from experiment. The result of this additional convolution is to smear intensity along the energy axis. For the LMTO calculations in figure 5(b) and 5(c) all the intensity lies within the free-electron-like parabola. The experiment by contrast has intensity away from this parabola.

A Monte Carlo (MC) simulation of the effects of elastic and inelastic multiple scattering present in the experimental results provides a deeper understanding of the structures in the measured intensity and allows one to make a more accurate determination of band parameters. A detailed description of the MC code can be found elsewhere[29]. The result is shown in figure 5(d). At least one ghost image of the conduction band parabola shifted by about 19 eV downward is observable. This is due to excitation of a first order plasmon in the beryllium layer. Elastic scattering processes introduce additional intensity most noticeably inside the parabola, i.e., the intensity is smeared along the momentum axes. There is qualitative agreement between the experiment and LMTO calculation provided both lifetime and multiple scattering are accounted for. The experimental background intensity is, however, higher than that predicted by the MC simulation. One cause of this discrepancy might be an inadequate description of the low energy loss processes.

For a quantitative comparison of the experimental and theoretical results we take slices through figure 5 along the binding energy axis to produce the binding energy plots

shown in figure 6. The first order plasmon and smooth background have been removed from figures 5(a) and 5(d) by fitting a Lorentzian and fourth order polynomial respectively. To improve statistics in the experimental result the positive and negative momentum halves of figure 5(a) have been summed. The momentum width of the binding energy plots is 0.1 a.u. Each set of data is normalized in the momentum interval where it reaches maximum intensity.

It is especially clear from figure 6 how dramatically lifetime broadening has changed the momentum dependence of peak heights. The LMTO peak has its maximum intensity in the 0 a.u. momentum interval and monotonically decreases in height and broadens as the momentum increases. The experimental intensity peaks in the 0.6 a.u. momentum interval, whereas the lifetime-broadened LMTO and MC simulation curves peak at 0.7 a.u momentum. The lifetime-broadened LMTO and MC simulation curves are very similar, indicating that the multiple scattering simulation does not significantly alter the conduction band parabola. Both of these curves reproduce the experimental peak heights very well up to a momentum of 0.8 a.u. At higher momentum the experimental peak decreases in height and broadens faster than the MC peak. This momentum range corresponds to the edge of the first Brillouin zone where other bands heavily contribute to the overall density. Dispersion of the experimental and theoretical peaks is different. All three theoretical curves show roughly the same dispersion, but disperse more rapidly in energy as the momentum increases when compared with experiment.

Although the behavior of peak heights is completely different after inclusion of the lifetime broadening, the peak areas remain nearly the same. This is clearly illustrated in figure 7, where the electron momentum density (EMD) derived from the curves of figure 6

by integration over binding energies are shown. All curves are normalized to unity. The two LMTO curves lie close to each other throughout the 2 a.u. momentum range and differ from the MC and experimental data. Multiple scattering smears the intensity along the momentum and energy axes in contrast to lifetime broadening where redistribution of the intensity occurs only in energy. For this reason at zero momentum the MC and experimental EMD's are only 0.85 and 0.8, respectively, slowly increasing to a maximum at 0.6 a.u. There is a difference of about of 0.05 between the experiment and MC curves at low momenta with a much more significant discrepancy in the momentum region from 0.85 to 1.05 a.u. A point of inflection in the MC and LMTO curves located at about 1.05 a.u. approximately marks the Fermi momentum k_F. This point is significantly lower in the experiment (0.9 a.u.). Above 1.1 a.u. the experiment and MC EMDs show a reasonable similarity. However, they are both above the LMTO curves in this momentum interval, again due to the effect of multiple scattering.

Figure 8 shows momentum profiles for experiment and MC simulation extracted from figure 5(a) and 5(d) by taking 1 eV slices along the momentum axis. Both data sets are normalized in the 9.34 eV momentum interval. The experimental peaks are systematically shifted to lower momentum compared to the MC result. A maximum shift of 0.15 a.u. occurs at the top of the band. The peak shapes and tails are similar, indicating our MC simulation gives an adequate description of small angle elastic scattering.

The density of occupied states (DOS) can be extracted from the experimental and theoretical data by integrating the momentum profiles. The results are shown in figure 9. The background has been subtracted for the experiment and MC data. This is important for the DOS because otherwise the result would be substantially deformed by the background at higher electron momenta q due to the phase space factor q^2 in the integration. Binding

energies refer to the Fermi level from the LMTO calculation (the conduction band minimum is at 10.43 eV). All curves are normalized to unity. The LMTO data convoluted with the experimental resolution shows a double peak structure at the top with a dip of about 0.3 at about 3 eV. After accounting for the finite hole lifetime this structure becomes much shallower. The MC curve is similar to the lifetime curve implying a good quality of the background subtraction in the MC data. The experimental curve is similar in shape to the MC curve, but without any structure around 3 eV. The only substantial deviation of the curves occurs at the top of the conduction band. The experimental density of states extends well beyond the Fermi level compared to MC. The residual experimental density is equal to about 0.6 at the Fermi level, whereas for MC this value is only 0.3. There are two possible causes or their combination for this disagreement: first, the experimental bandwidth is larger by about 1 eV than that predicted by LMTO and, second, the density of states in beryllium from the experiment is higher at the Fermi level than that predicted by LMTO. The former cause is in place as follow from the next section of the paper.

4.2. Band dispersion and Bandwidth

We have extracted dispersion relationships for the conduction band from binding energy and momentum profiles similar to those presented in figures 6 and 8 but with a finer binning using a fitting procedure. The complex shape of the binding energy peaks, especially evident at higher momenta, does not match a simple Gaussian or Lorentzian function. For this reason we fit only the top portion of the binding energy peaks using a Gaussian function to obtain the precise position of the peak maximum. Beyond the Fermi momentum k_F where

the binding energy profiles show broad structures instead of peaks we interpret the average energy of these structures as the dispersion relation.

The resulting dispersion curves are shown in figure 10. Binding energies are referenced to the vacuum level with the theoretical bands shifted by approximately 4 eV. The two sets of experimental points are close to each other in the 0.35 - 0.85 a.u interval. Outside this interval the momentum profiles could not be used to determine the dispersion relation due to flattening of the conduction band, in this case we relay only on data extracted from the binding energy profiles. The three theoretical dispersion curves lie close to each other showing a maximum deviation of about 1 eV at the Fermi momentum k_F. Convolution of the LMTO data with lifetime effects and MC simulation tends to broaden the dispersion curve. The experimental dispersion parabola is substantially narrower than any of the three theoretical curves. The deviation between the experimental and MC curves increases in magnitude as momentum increases reaching a maximum of about 1.5 eV at a momentum of 0.95 a.u. and 0.15 a.u. at an energy of 5 eV. The later value corroborates the difference noted earlier in the EMD curves of figure 7. A similar result was observed for our EMS measurement of Ca^{30}.

In the inset of figure 10 the mean energies of the conduction band intensity in the momentum range from 1 to 1.95 a.u. are shown. These values are extracted from binding energy profiles. One can see that while the LMTO energies disperse from about 5.5 to 10.5 eV the MC curve remains basically flat for momenta over 1.2 a.u. A possible cause of this flattening is intense elastic scattering in the target that effectively smears intensity along the momentum axis and the center of the smeared intensity remains at constant energy over a wide momentum interval. This constant value of 8.5 eV marks approximately the middle of

the theoretical band dispersion that further support the intense elastic scattering smearing of the band intensity in this momentum region. The experimental points show good agreement with the MC data. It is difficult to obtain any quantitative information concerning band dispersion in this high momentum region because of this smearing.

There are several ways to estimate the occupied bandwidth from our experiment data. We measure energies of the electrons relative to the vacuum level of the spectrometer and so the work function of the metal is needed to be able to reference energies to the Fermi level. Using the Be work function dependence from the oxygen exposure obtained by Gustafsson and his coworkers[31] and the data on the sticking coefficients for oxygen and water vapor from Zalkind *at el*[16] we have calculated an average value of 3.78 eV for the work function for our measured data. Taking into account the energy of the band minimum of 14.34 eV we get an estimate for the occupied bandwidth of 10.56 eV. This value is close to the LMTO value of 10.43 eV. This value represents the 'full' theoretical bandwidth independent of lifetime and multiple scattering effects.

An estimate of the bandwidth can also be extracted from the dispersion curves of figure 10 by taking the difference between the band top and bottom. The results for the experimental and MC dispersion curves give values of 9.51 ± 0.08 eV and 9.36 eV. The later value means a shrinking of 1.07 eV of the MC bandwidth compared to the original LMTO. So the 'full' experimental bandwidth is expected to be 10.58 ± 0.1 eV, which agree well with the previously obtained value.

Another method of the bandwidth determination is based on an evaluation of the work function of the spectrometer using the experimental and MC binding energy profiles at high momenta. Background subtracted binding energy profiles of the experiment and MC

integrated over the (0.8 - 2) a.u. momentum interval are shown in figure 11. The energy scale is referenced to the vacuum level of the spectrometer for the experiment and to the Fermi level for the theory. Both data sets are normalized to unity. Roughly speaking, the intensity at the low energy slope of both profiles is formed by electrons located near the Fermi surface. A shift of 3.2 ± 0.1 eV measured close to their bases gives the work function of the spectrometer. Despite the fact that this value is significantly less of the earlier calculated value of 3.78 eV it is more reliable as accounts for possible systematic errors present in the energy scale of our spectrometer, i.e. charging effects and calibration errors. It gives a bandwidth of 11.15 ± 0.15 eV, which is about 0.7 eV higher of that from the theory.

Other numerous theoretical investigations of the band structure of beryllium give a broad range for the bandwidth. Figure 12 shows results of some theoretical calculations and measurements. Open circles represent theoretical values and solid points are experimental ones. The free-electron gas model predicts a value of 14.14 eV[32]. A theoretical value of 10.6 eV was obtained by Cornwell[33] who used an interpolation scheme in the frame of pseudo-potential method and by Blaha *et al*[34] by means of the full-potential linearised-augmented-plane-wave method and on the basis of the local density approximation. Most calculations give bandwidths around 11-13 eV[1,5,2,6,35,39].

On the other hand, experimental measurements of the occupied bandwidth in metallic beryllium are quite scarce. Skinner[36] performed the first measurement of the K-emission spectrum of metallic beryllium and obtained a value of 13.8 ± 1 eV. Sagawa[37], using the same technique, obtained a value of 16.88 eV presumably without allowance for a long-wave tail in the spectrum. Lukirskii *et al*[38] obtained a value of 10.25 ± 0.5 eV, which is close to our result. A more recent measurement of the energy of the $\tilde{A}_1^+$ symmetry point relative to

the Fermi level was made by Jensen *et al*[39] using ARPES. They obtained a value of 11.1 ± 0.1 eV, which agrees perfectly with our value.

5. Conclusion

We have measured the full energy and momentum resolved electronic structure of the conduction band of beryllium by means of electron momentum spectroscopy. We have also compared the obtained experimental results to band structures calculated within the full potential linear muffin-tin orbital approximation. Band dispersions have been extracted from the experimental and theoretical data.

The dispersion curve looks similar to that of a free-electron metal. Comparison of theory (after MC application) and experiment shows good general agreement of peak intensities in the binding energy and momentum profiles. However, band dispersions extracted those profiles exhibit a continuous deviation from each other as momentum increases, the experimental curve being narrower by 0.15 a.u. near the Fermi momentum k_F. The measured conduction bandwidth is larger as much as 0.7 eV than that of the theory but agrees well with some other experimental and theoretical data.

Acknowledgments

This work was supported by grants from the Australian Research Council and Flinders University. One of the authors (MAB) received support from the Shahid Bahonar University, Kerman, Iran, which allowed him to participate in this experiment. The authors

acknowledge Prof. I E McCarthy for providing the scattering cross-sections used in the Monte Carlo procedure.

FIGURE CAPTIONS

Figure 1. Layout of (a) the scattering geometry, and (b) target orientation with respect to incident and two outgoing electrons. The shaded sectors of cones in (a) designate the angular acceptance of the analyzers. The shaded layer in (b) represents the portion of the target that contributes most to the measured energy-momentum density.

Figure 2. Auger spectrum *N(E)* of the beryllium target (a) and differential d*N(E)*/d*E* spectrum (b) immediately after deposition.

Figure 3. Electron energy loss spectra for a 3 nm Be film deposited onto a 3 nm am-C substrate (a) for the 19.6 keV fast electrons and (b) the 1.2 keV slow electrons. In (a) solid lines present a fit decomposition of the loss structure due to surface and bulk plasmon excitations in beryllium, dash line is due to bulk plasmon loss in am-C. In (b) solid lines show a fit result for the first and second order bulk plasmon losses in beryllium.

Figure 4. Band dispersions (top row) and electron momentum densities for Be calculated within the FP-LMTO approximation along several high symmetry directions.

Figure 5. Binding energy-momentum resolved densities of metallic Be, (a) measured by EMS, (b) calculated within the FP-LMTO scheme, spherically averaged and convoluted with instrumental resolution, (c) the same as (b) but additionally broadened to account for the experimentally determined hole lifetimes, (d) simulated by the Monte Carlo procedure using

the density in (c) as input. The energy scales in (b), (c) and (d) have been shifted by approximately 4 eV to match the experimental binding energy referenced to the vacuum level. Intensity is on a linear gray scale: the darker color the higher intensity.

Figure 6. Background subtracted binding energy peak profiles for beryllium integrated over 0.1 a.u. momentum intervals from the experiment (points with error bars) and the Monte Carlo simulation (solid lines). Dashed lines stand for LMTO binding energy peak profiles: convoluted with instrumental resolution (short dashes) and additionally lifetime broadened (long dashes). All curves have been shifted by approximately 4 eV to match the experiment referenced to the vacuum level.

Figure 7. Electron momentum density for beryllium extracted from the binding energy profiles from the experiment (points with error bars), Monte Carlo simulation (solid lines), LMTO convoluted with instrumental resolution (short dash line) and LMTO additionally lifetime convoluted (long dash line). All data sets are normalized to unity. The arrow marks the position of the Fermi momentum k_F.

Figure 8. Momentum profiles for beryllium integrated over 1 eV energy intervals from the experiment (points with error bars) and the Monte Carlo (MC) simulation (solid lines). Both sets of data have been normalized in the 9.34 eV momentum profile. The MC curves have been shifted by approximately 4 eV to match the experiment referenced to the vacuum level.

Figure 9. Density of occupied states for the conduction band of beryllium extracted from the momentum profiles. Points with error bars are the experimental data, solid line is the Monte Carlo simulation, short dash line is the LMTO prediction convoluted with instrumental resolution and long dash line is the LMTO prediction additionally lifetime convoluted. All data sets are normalized to unity. Binding energy is relative to the Fermi level.

Figure 10. In (a) conduction band dispersions for beryllium derived from the experiment and theory. Full points with vertical error bars, solid line, long and short dashed lines line are derived from the binding energy profiles of the experiment, the Monte Carlo simulation, LMTO convoluted with instrumental resolution and LMTO additionally lifetime convoluted, respectively. Open points with horizontal error bars are derived from the experimental momentum profiles. Inset shows a higher momentum extension of the band dispersion. Binding energy is relative to the vacuum level. The arrow marks the position of the Fermi momentum k_F.

Figure 11. Background subtracted binding energy profiles for beryllium integrated over the (0.8 - 2) a.u. momentum interval for the experiment (full points) and the Monte Carlo simulation (solid line). The energy is referred to the vacuum for the experiment and to the Fermi level for the Monte Carlo. Intensities are normalized to unity. The indicated shift of 3.2 ± 0.1 eV is related to the work function of the spectrometer.

Figure 12. Historic retrospective of some results obtained for the occupied bandwidth (in eV) in beryllium. Full points with error bars present experimental data, open points are theoretical predictions. Horizontal line is a free electron gas value.

References

[1] S. T. Inoue and J. Yamashita, J. Phys. Soc. Jpn. **35**, 677 (1973).
[2] M. Y. Chou, P. K. Lam and M. L. Cohen, Phys. Rev. **B28**, 4179 (1983).
[3] P. J. Brown, Phil. Mag. **26**, 1377 (1972).
[4] G. Loupias, J. Petiau, A. Issolah and M. Schneider, Phys. Stat. Sol. (b) **102**, 79 (1980); N. K. Hansen, P. Pattison and J. R. Schneider, Z. Phys. **B35**, 215 (1979); R. Currat, P. D. DeCicco and R. Kaplow, Phys. Rev. **B3**, 243 (1971); W. C. Phillips and R. J. Weiss, Phys. Rev. **171**, 790 (1968).
[5] T. L. Loucks and P. H. Cutler, Phys. Rev. **133**, A819 (1964).
[6] C. Herring and A. G. Hill, Phys. Rev. **58**, 132 (1940).
[7] Siegbahn and Magnusson, Z. Phys. **87**, 291 (1934); Siegbahn and Magnusson, Z. Phys. **96**, 1 (1935).
[8] O'Bryan and Skinner, Phys. Rev. **45**, 370 (1934).
[9] E. Jensen, R. A. Bartynski, T. Gustafsson, E. W. Plummer, M. Y. Chou, M. L. Cohen and G. B. Hoflund, Phys. Rev. **B30**, 5500 (1984).
[10] S. A. Canney, M. J. Brunger, I. E. McCarthy, P. J. Storer, S. Utteridge, M. Vos and E. Weigold, J. Electron Spectrosc. Relat. Phenom. **83,** 65 (1997); P. Storer, R. S. Caprari, S. A. C. Clark, M. Vos and E. Weigold, Rev. Sci. Instrum. **65,** 2214 (1994).
[11] M. A. Coplan, J. H. Moore and J. P. Doering, Rev. Mod. Phys. **66,** 985 (1994); I. E. McCarthy and E. Weigold, Rep. Prog. Phys. **54,** 789 (1991); I. E. McCarthy and E. Weigold, Rep. Prog. Phys. **51,** 229 (1988).
[12] V. G. Neudatchin, V. G. Levin and Yu. F. Smirnov, Nucl. Sci. Appl. **1**, 277 (1981).
[13] S. J. Utteridge, V. A. Sashin, S. A. Canney, M. J. Ford, Z. Fang, D. R. Oliver, M. Vos and E. Weigold, App. Surf. Sci. **162-163,** 357 (2000); Z. Fang, X. Guo, S. Utteridge, S. A. Canney and I. E. McCarthy, Rev. Sci. Instrum. **68,** 4396 (1997).
[14] S. A. Canney, V. A. Sashin, M. J. Ford and A. S. Kheifets, J. Phys.: Condens. Matter **11,** 7507 (1999).
[15] V. A. Sashin, H. E. Dorsett, M. A. Bolorizadeh and M. J. Ford, J. Chem. Phys **113**, 8175 (2000).
[16] S. Zalkind, M. Polak and N. Shamir, Surf. Sci. **385**, 318 (1997).
[17] M. Suleman and E. B. Pattinson, J. Phys. F: Metal Phys. **1,** L24 (1971); R. J. Fortner and R. G. Musket, Surf. Sci. **28,** 339 (1971).
[18] D. M. Miliotis, Phys. Rev. **B3**, 701 (1971).
[19] C. J. Powell, Proc. Phys. Soc. **76,** 593 (1960).
[20] A. M. Bradshaw and W. Wyrobisch, J. Electron. Spectrosc. Relat. Phenom. **7**, 45 (1975).
[21] N. Swanson, J. Opt. Soc. Amer. **54,** 1130 (1964); T. Aiyama and K. Yada, J. Phys. Soc. Jpn. **36,** 1554 (1974).
[22] H. Höchst, P. Steiner and S. Hüfner, Phys. Lett. **60A**, 69 (1977).
[23] P. Steiner, H. Höchst and S. Hüfner, Z. Phys. **B30**, 129 (1978).
[24] J.J. Quinn, Phys. Rev. **126**, 1453 (1962).
[25] A. S. Kheifets , D. R. Lun and S. Y. Savrasov 1999 *J. Phys.: Condens. Matter* **11** 6779
[26] R. Wyckoff 1963 *Crystal Structures* (New York: Interscience)
[27] B. I. Lundqvist, Phys. Stat. Sol. **32**, 273 (1969).
[28] V. A. Sashin, S. A. Canney, M. J. Ford, M. Bolorizadeh, D. R. Oliver and A. S. Kheifets, J. Phys.: Condens. Matter **12,** 125 (2000).
[29] M. Vos and M. Bottema, Phys. Rev. **B54**, 5946 (1996).
[30] V.A. Sashin, M.A. Bolorizadeh, A.S. Kheifets and M.J. Ford, J. Phys.: Condens. Matter **12**, 9407 (2000).
[31] T. Gustafsson, G. Brodén and P. Nilsson, J. Phys. F: Metal Phys. **4**, 2351 (1974).
[32] C. Kittel, Introduction to Solid State Physics, (John Wiley & Sons, Inc., New York, Chichester, Brisbane, Toronto, Singapore), 1996.
[33] J. F. Cornwell, Proc. Roy. Soc. **A261**, 551 (1961).
[34] P. Blaha and K. Schwarz, J. Phys. F: Metal Phys. **17**, 899 (1987).
[35] R. Jacques, Cahiers Phys. **70**, 1 (1956); R. Jacques, Cahiers Phys. **71-72**, 31 (1956); J. H. Terrell, Phys. Rev. **149**, 526 (1966); M. Taut, Phys. Stat. Sol. (b) **54**, 149 (1972); P. O. Nilsson, G. Arbman and T. Gustafsson, J. Phys. F: Metal Phys. **4**, 1937 (1974); L. Wilk, W. R. Fehlner and S. H. Vosko, Can. J. Phys. **58**, 266 (1978).
[36] H. W. B. Skinner, Phil. Trans. Roy. Soc. (London) **A239**, 95 (1946).
[37] T. Sagawa, Sci. Rep. Tôhoku Univ. (I) **45**, 232 (1961).
[38] A. P. Lukirskii and I. A. Brytov, Sov. Phys. – Solid State **6**, 33 (1964).

[39] E. Jensen, R. A. Bartynski, T. Gustafsson, E. W. Plummer, M. Y. Chou, M. L. Cohen and G. B. Hoflund, Phys. Rev. **B30**, 5500 (1984).

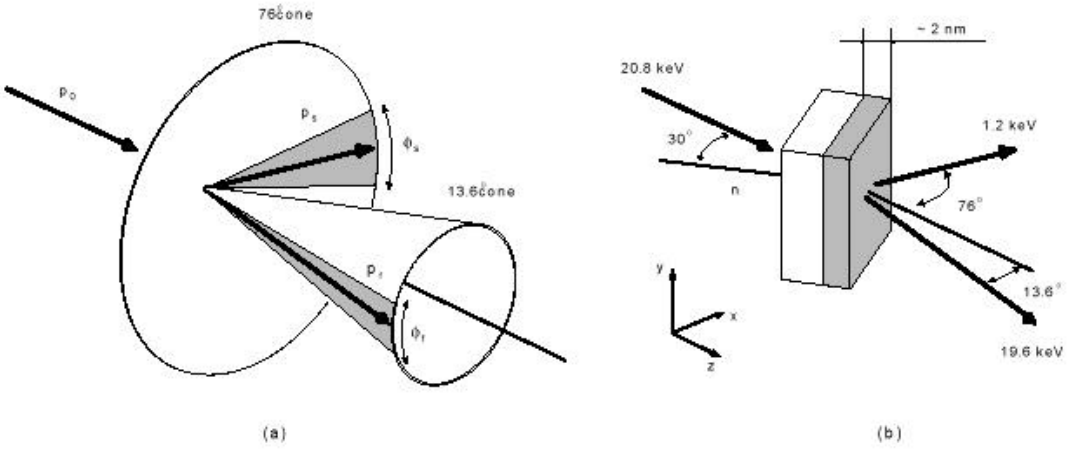

Fig. 1

Fig. 2

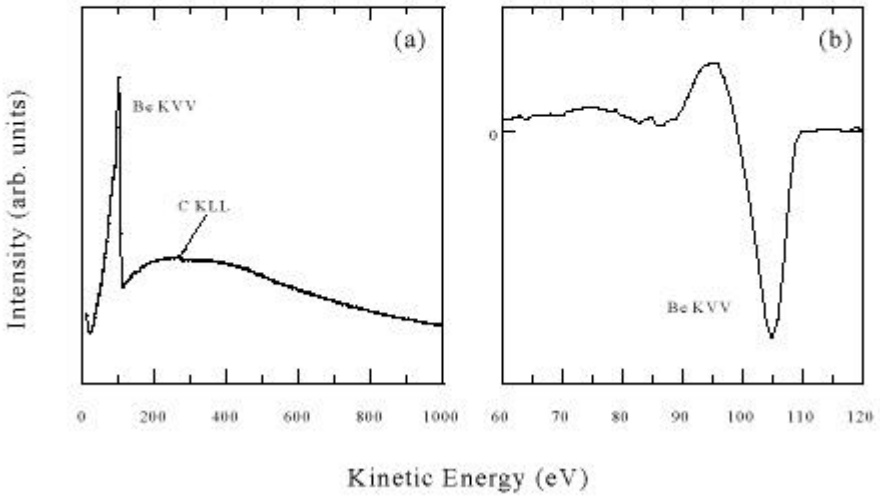

Fig. 3

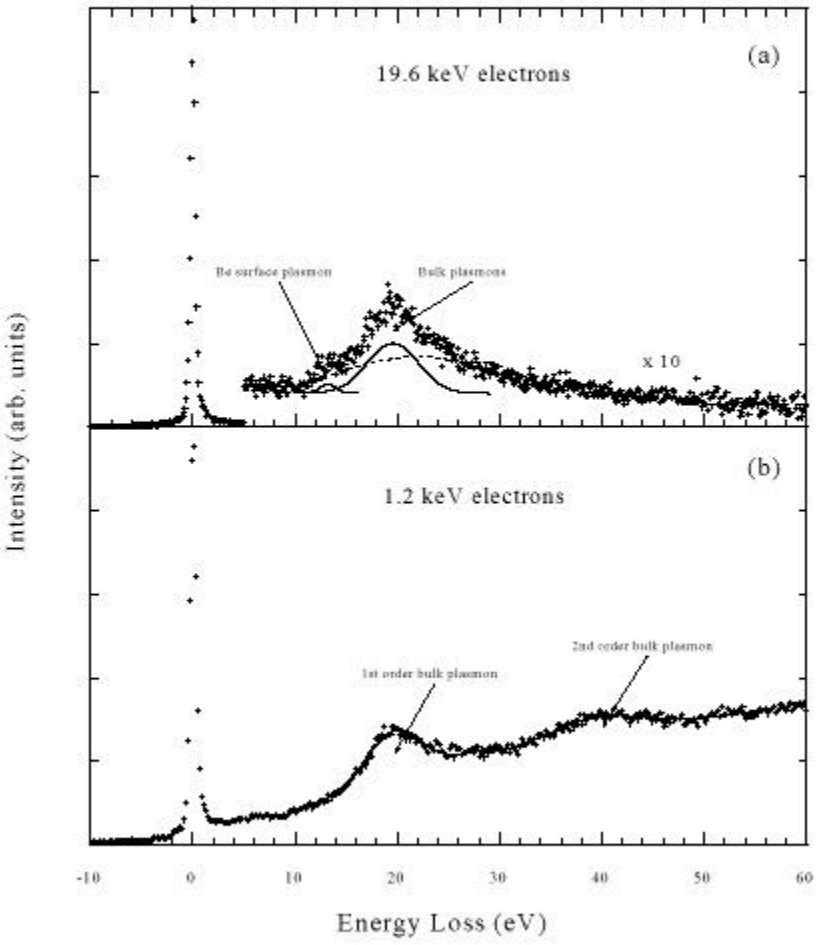
(a)
19.6 keV electrons
Be surface plasmon
Bulk plasmons
x 10
(b)
1.2 keV electrons
1st order bulk plasmon
2nd order bulk plasmon
Intensity (arb. units)
-10
0
10
20
30
40
50
60
Energy Loss (eV)

Fig. 4

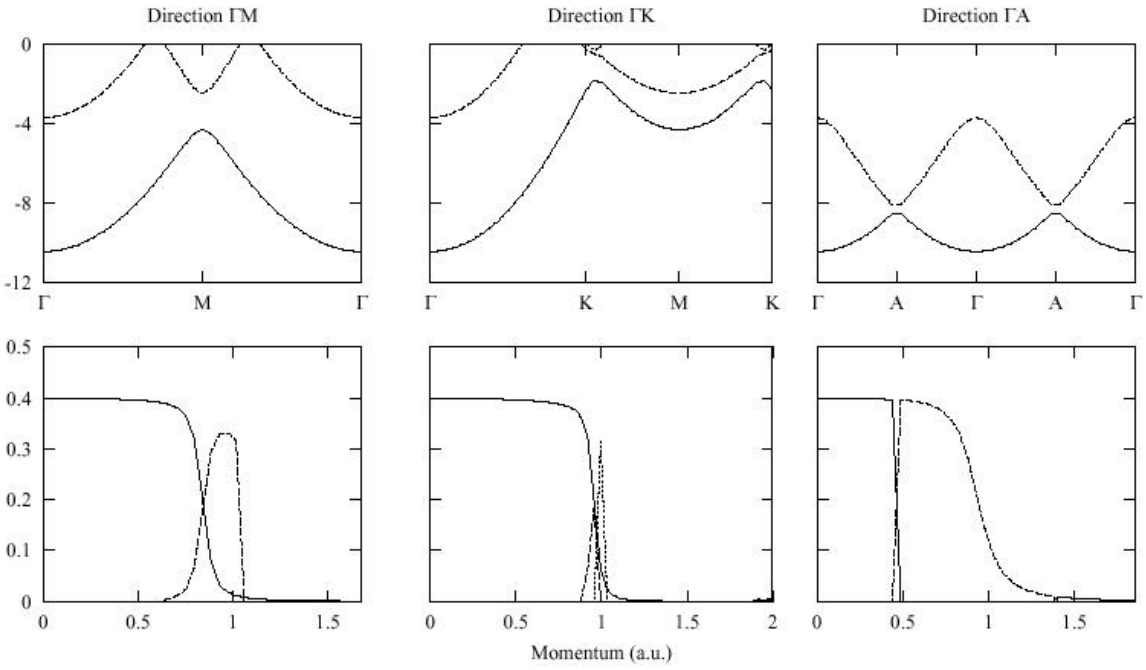
Direction ΓM
Direction ΓK
Direction ΓA
0
-4
-8
-12
Γ
M
Γ
Γ
K
M
K
Γ
A
Γ
A
Γ
0.5
0.4
0.3
0.2
0.1
0
0
0.5
1
1.5
0
0.5
1
1.5
2
0
0.5
1
1.5
Momentum (a.u.)

Fig. 5

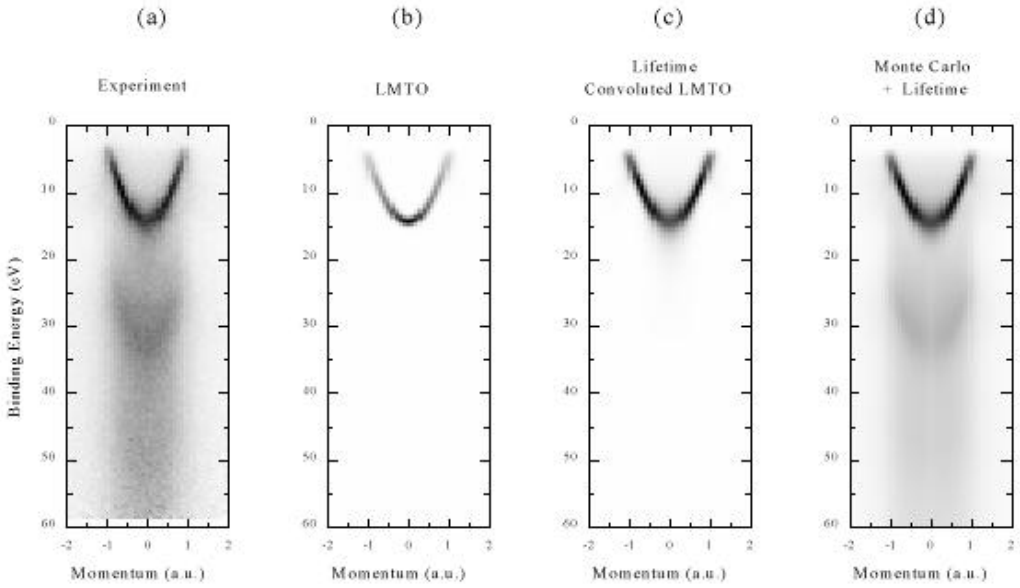
(a)
Experiment
(b)
LMTO
(c)
Lifetime
Convoluted LMTO
(d)
Monte Carlo
+ Lifetime
Binding Energy (eV)
0
10
20
30
40
50
60
-2
-1
0
1
2
Momentum (a.u.)

Fig. 6

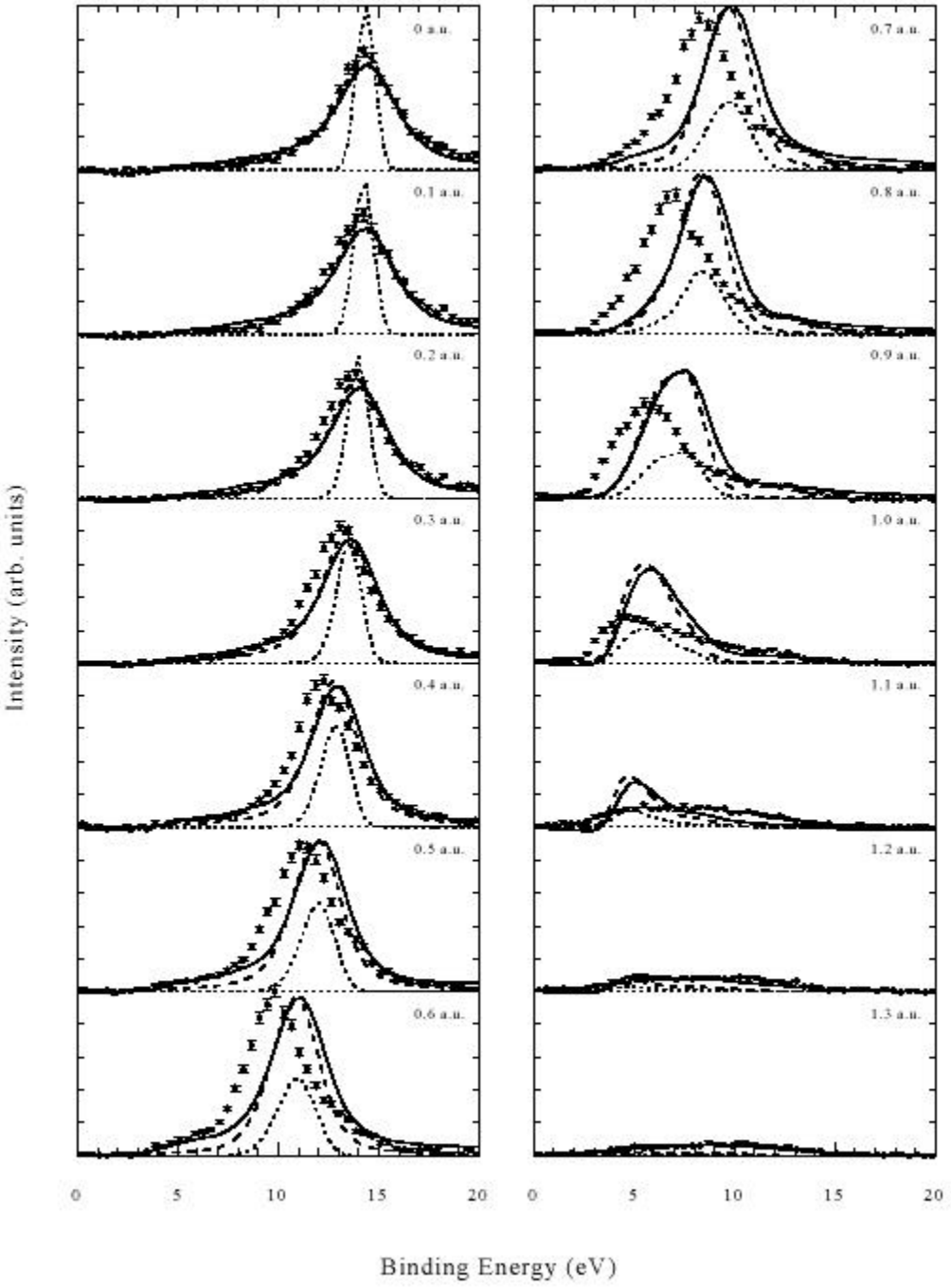
0 a.u.
0.1 a.u.
0.2 a.u.
0.3 a.u.
0.4 a.u.
0.5 a.u.
0.6 a.u.
0.7 a.u.
0.8 a.u.
0.9 a.u.
1.0 a.u.
1.1 a.u.
1.2 a.u.
1.3 a.u.
0
5
10
15
20
Intensity (arb. units)
Binding Energy (eV)

Fig. 7

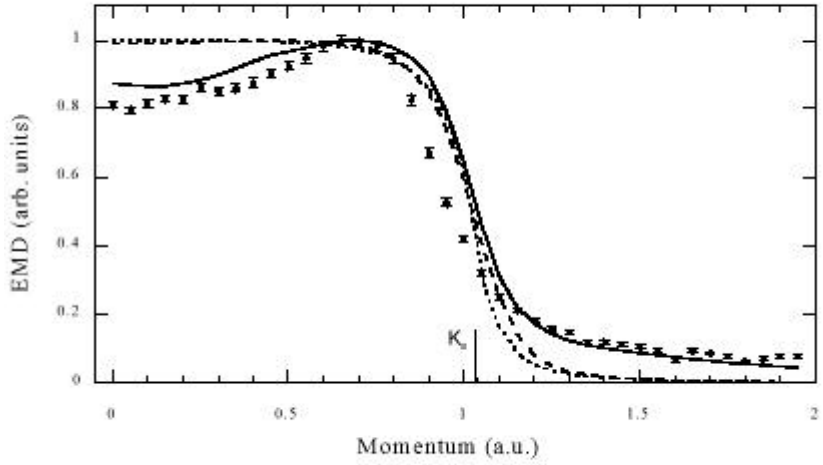

Fig. 8

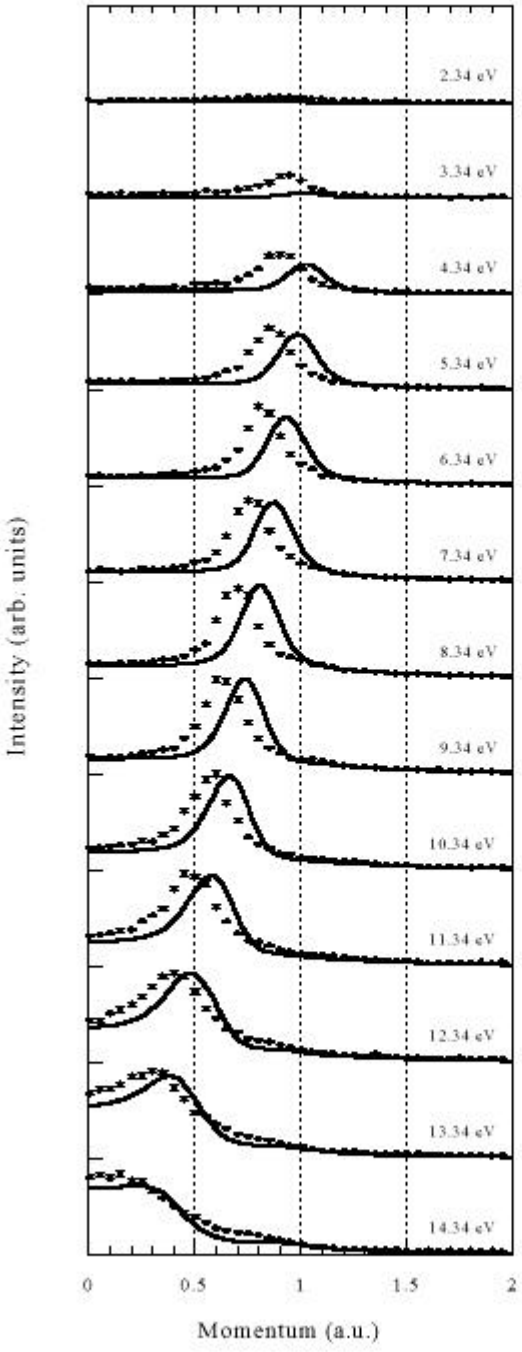
2.34 eV
3.34 eV
4.34 eV
5.34 eV
6.34 eV
7.34 eV
8.34 eV
9.34 eV
10.34 eV
11.34 eV
12.34 eV
13.34 eV
14.34 eV
Intensity (arb. units)
0
0.5
1
1.5
2
Momentum (a.u.)

Fig. 9

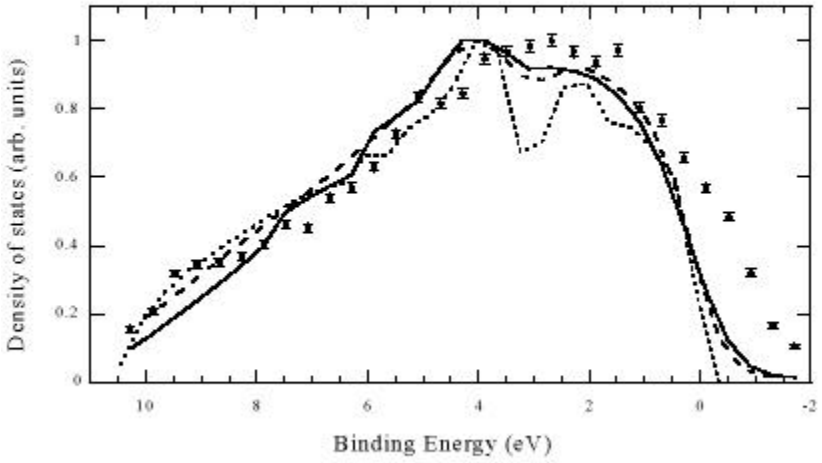
Density of states (arb. units)
Binding Energy (eV)

Fig. 10

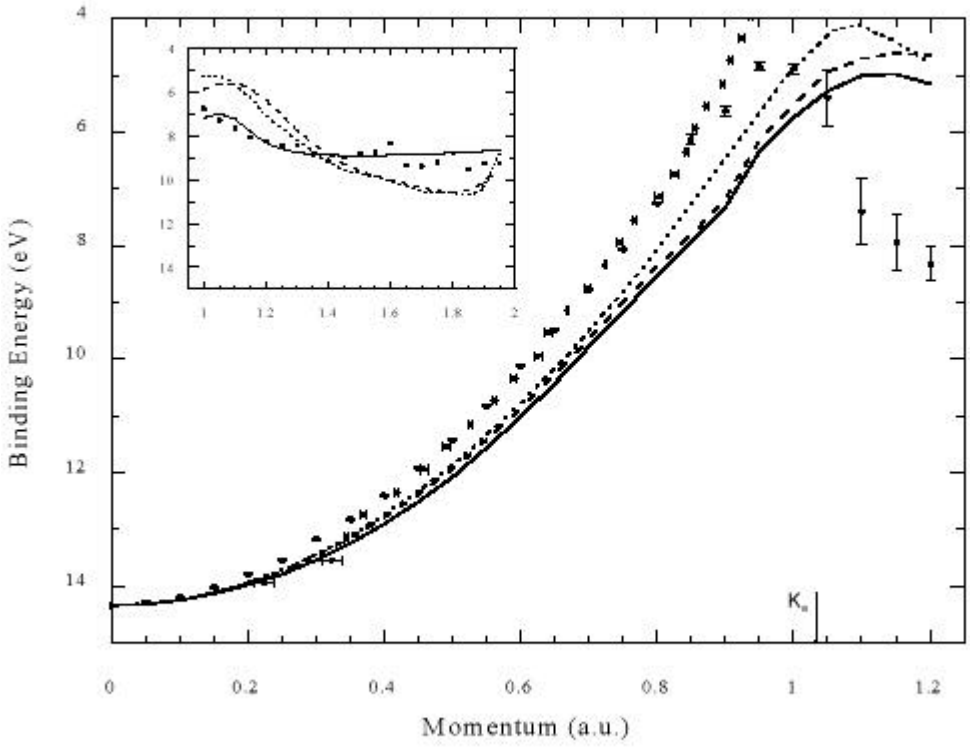
Binding Energy (eV)
Momentum (a.u.)
K

Fig. 11

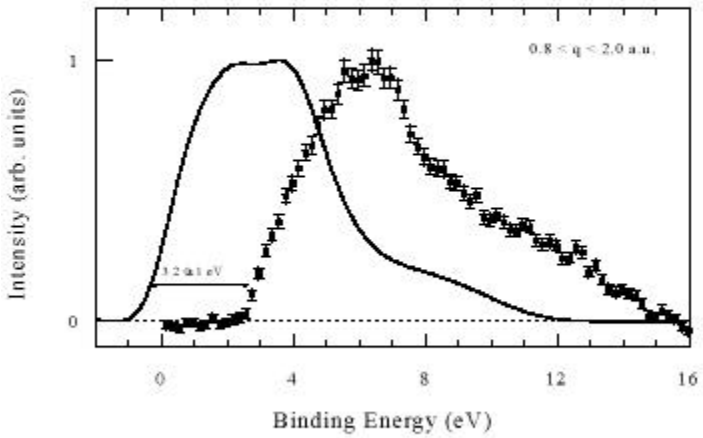
0.8 < q < 2.0 a.u.
1.2±0.1 eV
Intensity (arb. units)
1
0
0
4
8
12
16
Binding Energy (eV)

Fig. 12

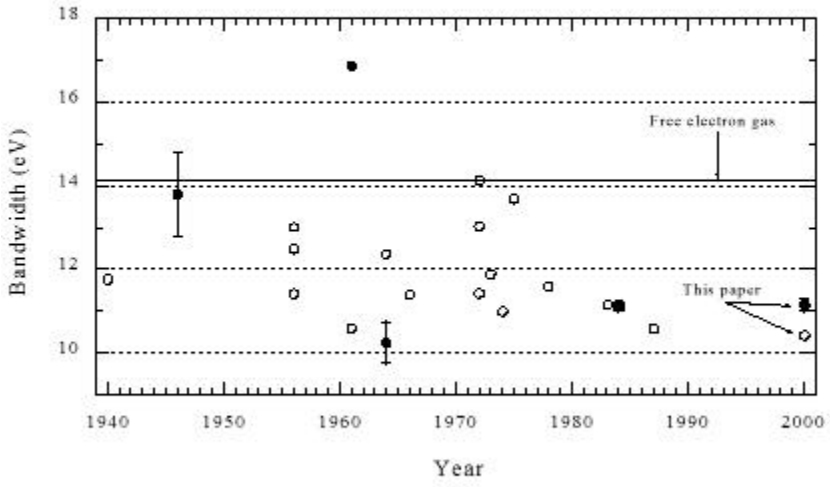
Bandwidth (eV)
18
16
14
12
10
Free electron gas
This paper
1940
1950
1960
1970
1980
1990
2000
Year